communications chemistry

A Nature Portfolio journal

Article

https://doi.org/10.1038/s42004-025-01554-7

Selective manipulation of L-cysteine crystal polymorphs using focused laser beams

Hozumi Takahashi [1] ✉, Hiroshi Y. Yoshikawa [1] & Teruki Sugiyama [2,3] ✉

The selective manipulation of crystal polymorphs holds profound implications across diverse scientific and industrial fields, as distinct polymorphs exhibit unique physical and chemical properties. This study demonstrates selective polymorphic manipulation by laser trapping – a technique enabling contactless manipulation and condensation of matter at the nanometer-scale and micrometer-scale. L-cysteine, a ubiquitous amino acid employed in pharmaceuticals and food additives, was targeted. We reveal that continuous-wave laser irradiation yields single crystals of the metastable polymorph, whereas continued irradiation with high-repetition-rate femtosecond laser pulses induces poly-crystallization of the stable form. Crucially, by strategically alternating between these two laser modalities during crystal growth, we can open up new crystallization pathways, including the single crystal growth of the stable phase. These findings underscore the significant potential of focused laser beams for precision polymorphic engineering, paving the way for the development of advanced materials with tailored properties.

Crystal polymorphism—the ability of a material to exist in more than one crystalline form—has garnered significant attention across diverse scientific and industrial fields due to the distinct physical and chemical properties exhibited by different polymorphs. In the pharmaceutical sector, for instance, polymorphism profoundly influences critical drug characteristics such as solubility, stability, and bioavailability, all of which directly impact the drug's efficacy and safety[1,2]. Similarly, in materials science, polymorphism affects the mechanical, optical, and electronic properties of materials, influencing the performance of semiconductors, pigments, and energetic materials[3–5]. Consequently, developing effective strategies for the precise control of crystal polymorphs is crucial for designing crystalline materials with tailored properties. Traditionally, polymorphic control has been achieved by adjusting environmental parameters such as temperature, concentration, and solvent[6]. However, controlling the polymorphism of organic compounds is challenging due to the relatively weaker intermolecular forces driving their crystallization, such as van der Waals and hydrogen bonding. Even with a systematic screening of environmental parameters, the precise and reproducible preparation of the desired number of crystals and crystal polymorphs in organic compounds often remains difficult.

Recent research has focused on the physical aspects of laser irradiation, such as electric field effects and heat generation, as a promising external perturbation for controlling the crystallization of various organic compounds[7–10]. Laser-based techniques such as non-photochemical laser-induced nucleation (NPLIN) and laser ablation have shown potential in achieving polymorphic control, particularly in amino acids and pharmaceutical compounds[11–18]. Recent studies suggest that crystal nucleation and polymorphic selectivity through these methods are attributed to photothermally and/or photochemically produced bubbles, which locally increase solute concentrations and/or enhance heterogeneous nucleation[18–20].

Laser trapping, a technique that allows for the contactless manipulation and condensation of substances at the nanometer- and micrometer-scales[21–24], has also emerged as a potential tool for the precise control of crystallization events[25]. Studies have demonstrated that focused irradiation with continuous-wave (CW) laser at the air/solution interface can induce crystal formation without bubble generation, and the polymorphs of the resulting crystals are highly dependent on laser parameters (laser intensity, polarization mode) as well as environmental conditions (e.g., initial concentration)[26–28]. In terms of its mechanism, optical force, arising from the interaction between the laser's electric field and solutes (theoretically, treatment is summarized in Supplementary Note 1), plays a crucial role in condensing the solutes at/around laser focus[25,29]. Interestingly, utilizing a high-repetition-rate femtosecond (HRR fs) laser instead of a CW laser can induce not only trapping effects but also bubble generation[30,31], a

[1]Graduate School of Engineering, Osaka University, Suita, Osaka, Japan. [2]Department of Applied Chemistry and Center for Emergent Functional Matter Science, National Yang Ming Chiao Tung University, Hsinchu, Taiwan. [3]Division of Materials Science, Nara Institute of Science and Technology, Ikoma, Nara, Japan. ✉e-mail: h.takahashi@eei.eng.osaka-u.ac.jp; sugiyama@nycu.edu.tw

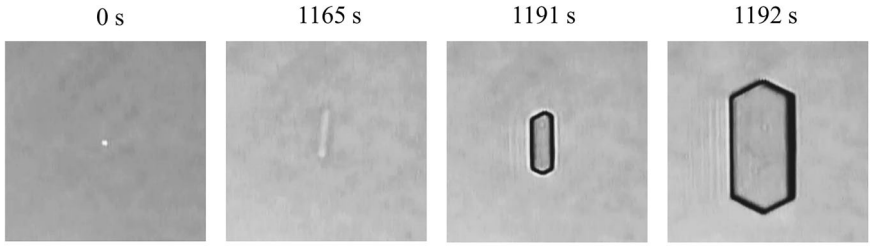

Fig. 1 | Dynamics of CW laser trapping-induced L-Cys crystallization. Representative crystallization behavior of L-Cys under CW laser trapping conditions. The laser intensity was set to 120 MW cm^{-2}. The scale bar represents 10 μm. A white spot shown at ~0 s is a focused 532 nm laser used as an indicator of the air/solution interface.

phenomenon often observed in studies of NPLIN and laser ablation[7,32]. This bubble generation contributes to polymorphic control in several compounds[30,31]. While the condensation of solutes through trapping effects is likely essential for inducing crystal nucleation[29,33], the critical factor governing polymorphic control remains elusive. Further investigation is necessary to achieve precise polymorphic manipulation.

In this study, we investigated polymorph control in L-cysteine (L-Cys), an amino acid commonly used in pharmaceuticals and food additives[34], by employing focused irradiation with CW and HRR fs lasers. L-Cys has also served as a model compound for polymorphic investigations[35–38]. Our findings revealed that CW laser trapping exclusively induced the crystallization of the α-form (metastable phase), while HRR fs laser trapping consistently yielded the crystallization of the β-form (stable phase). Additionally, we introduced an approach for single-crystal growth by strategically switching between CW and HRR fs laser irradiation during the crystallization process. This technique allows for precise manipulation of the polymorphic outcome and paves the way for the controlled growth of L-Cys single crystals with desired properties.

Results and discussion

Effects of CW laser irradiation on L-Cys crystallization

A near-infrared CW laser with a wavelength (λ) of 1064 nm was focused at the air/solution interface of an unsaturated L-Cys/D_2O solution with a supersaturation value of 0.84 (also see Methods). Here, the saturation value (SS) was defined as the C/C_e, where C and C_e are the concentration of the sample and the saturated concentration (1.16 mol kg^{-1} at 25 °C, Supplementary Note 2, and Supplementary Fig. 1), respectively. Figure 1 and Supplementary Movie S1 show the crystallization behavior of L-Cys under CW laser trapping. We adjusted the focal spot to the air/solution interface under the guidance of the reflection of the incident lasers (white dot at $t = 0$ s). No discernible changes were observed immediately after laser irradiation. After several tens of minutes, a thin, rod-like crystal was formed at the laser focus ($t = 1165$ s), subsequently developing into a hexagonal crystal with continued laser irradiation ($t \geq 1191$ s). The polymorphs of the generated L-Cys crystals were characterized by Raman spectroscopy (cf. Supplementary Note 3 and Supplementary Fig. 2). Throughout the crystallization process ($t \geq 1165$ s), Raman spectra confirmed the consistent presence of the α-form. Previous studies of polymorphism control using laser trapping have indicated the significant influence of laser parameters such as intensity and polarization on crystal polymorphs, crystallization probability, and induction time[26,27]. Therefore, we investigated the dependence of these parameters on the intensity of the linearly polarized CW laser. In this study, crystallization probability was defined as the ratio of successful trials, where crystal formation was observed within 40 min of laser irradiation, to the total number of trials. For example, if crystal formation was observed for 8 samples out of 10 trials, the crystallization probability would be 80%. To properly evaluate the tendency of the induction time, if crystallization was not observed within 40 min, the induction time was recorded as 40 min, indicating that the actual induction time is equal to or greater than 40 min. Figure 2 summarizes the results. Reliable L-Cys crystallization was always observed at a laser intensity of 120 MW cm^{-2} and higher, while crystallization was sometimes observed at 73 MW cm^{-2}. The induction time exhibited a decreasing trend with increasing laser intensity. This observation regarding the induction time was statistically validated through the Kruskal–Wallis test[39], which confirmed the significance of the difference ($H = 20$, $P = 0.0049\%$). Notably, despite variations in both crystallization probability and induction time, L-Cys crystals generated via CW laser trapping consistently exhibited the α-form. This exclusive formation of the α-form persisted across various conditions, including different polarization modes at 120 MW cm^{-2} (Supplementary Fig. 3) and a systematic screening of solution concentrations from 0.98 to 1.35 mol kg^{-1} (SS = 0.98–1.16), all of which consistently resulted in α-form crystallization. Although further systematic investigation of laser parameters and solution conditions may potentially enable the crystallization of stable β-form crystallization[38], our results indicate that CW laser trapping favors the formation of metastable α-form L-Cys crystals.

It is widely known that supersaturation plays a critical role in determining the polymorphic outcome of crystallization. As supersaturation is governed by both temperature and concentration, it is crucial to estimate the increase in both under CW laser trapping conditions to elucidate the mechanism underlying the exclusive formation of the metastable α-form. To observe the temporal evolution of concentration under laser trapping, we employed Raman spectroscopy to monitor the concentration dynamics of L-Cys. The L-Cys/D_2O solution exhibits several peaks between 200 and 2000 cm^{-1} (Supplementary Fig. 4a), and the intensity of some peaks (e.g., ~690, ~1430, and ~1870 cm^{-1}) was confirmed to be proportional to the L-Cys concentration. We tracked the concentration using the highest peak at ~1870 cm^{-1} (calibration curve: Supplementary Fig. 4b), which allowed for rapid measurement of Raman intensity (5 s per spectrum). Figure 3a shows the representative temporal evolution of Raman intensity at different laser intensities (73, 120, and 170 MW cm^{-2}). The intensity initially increased linearly with irradiation time, irrespective of the laser intensity. The intensity suddenly jumped upon crystallization, possibly facilitating the estimation of nucleation timing. The slope of the linear fitting curve before crystallization was $(0.55 \pm 0.12) \times 10^{-3}$ a.u. s^{-1} at 73 MW cm^{-2}, $(1.24 \pm 0.18) \times 10^{-3}$ a.u. s^{-1} at 120 MW cm^{-2}, and $(2.28 \pm 0.16) \times 10^{-3}$ a.u. s^{-1} at 170 MW cm^{-2}. From the calibration curve (Supplementary Fig. 4b), the concentration increase rates were 0.6 ± 0.1 mmol kg^{-1} s^{-1} at 73 MW cm^{-2}, 1.4 ± 0.2 mmol kg^{-1} s^{-1} at 120 MW cm^{-2}, and 2.5 ± 0.2 mmol kg^{-1} s^{-1} at 170 MW cm^{-2} (Fig. 3b, left axis), with significant differences confirmed by the Kruskal–Wallis test ($H = 13$, $P = 0.19\%$). These differences explain the observed shorter induction time at higher laser intensities (Fig. 2). Unexpectedly, despite the varying rates of concentration increase, the actual concentration of L-Cys at the point of crystallization, as estimated from the Raman intensity at the intersection of the linear fitting curves before and after crystallization, was consistently around 2.5 mol kg^{-1} for all laser intensities, with no significant differences ($H = 1.1$, $P = 57\%$). This remarkable consistency reveals a critical threshold for supersaturation that must be attained to initiate the formation of the α-form, regardless of how quickly that supersaturation level is reached.

Next, to accurately assess the supersaturation and its impact on the polymorphic outcome, we need to consider the effect of temperature elevation on L-Cys solubility. It is also essential to estimate the local temperature increase caused by laser irradiation, particularly since, for L-Cys, temperature influences which polymorph is formed (transition temperature: >32 °C, cf. Supplementary Note 3). Therefore, we investigated the

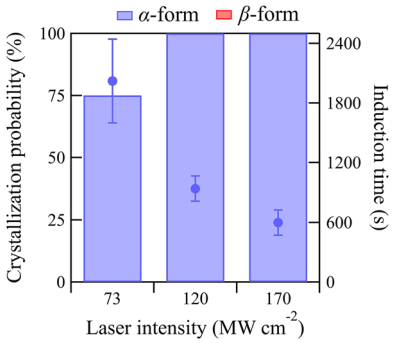

Fig. 2 | Impact of CW laser trapping on L-Cys crystallization. Influence of CW laser intensity on L-cysteine crystallization probability and induction time. Linearly polarized light was used, and eight samples were tested at each laser intensity. Blue bars represent crystallization probability (%), defined as the percentage of trials resulting in crystal formation within 40 min of laser irradiation. Blue dots indicate the induction times for each laser intensity. The error bars represent the standard deviation.

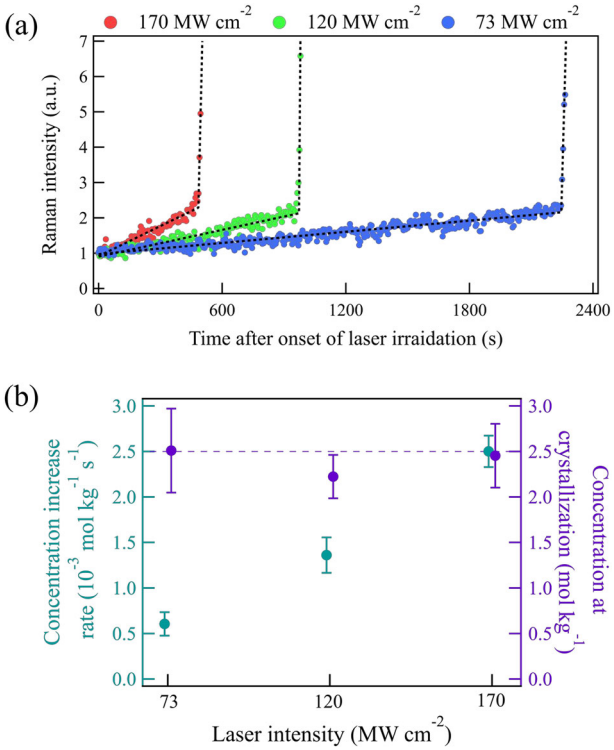

Fig. 3 | Concentration dynamics of L-Cys during CW laser trapping monitored by Raman spectroscopy. a Representative temporal evolution of Raman intensity under various laser intensities. The dashed lines represent the linear fitting curves before and after crystal nucleation. Raman spectra were acquired every 5 s. The laser power of the excitation laser was set to ~0.1 W (49 MW cm^{-2}). **b** Dependence of the concentration increase rate (left axis, turquoise blue) and concentration at the time of nucleation (right axis, purple) on laser intensity ($n = 5$). The marks are slightly offset along the horizontal axis to avoid overlapping. The error bars represent the standard deviation.

temperature elevation of the L-Cys/D_2O solution upon CW laser irradiation. Based on the spectroscopic analysis (Supplementary Note 4 and Supplementary Fig. 5), the temperature elevation coefficient at the laser focus was determined to be 1.3 °C W^{-1}. Consequently, in the laser intensity regime in this study, the maximum temperature elevation was estimated to be ~2 °C (25 °C → 27 °C). Since this achieved temperature is considerably lower than the transition temperature (>32 °C), we concluded that temperature elevation from laser irradiation should not contribute to the exclusive crystallization of the α-form. Hence, we focused on calculating the supersaturation at the point of crystallization. According to a previous study[40], a temperature increase from 25 °C to 27 °C leads to a 4% increase in L-Cys solubility in H_2O (see Supplementary Note 5). Assuming that the solubility in D_2O also increases by 4%, the supersaturation at crystallization was estimated to be SS = 2.5 [mol kg^{-1}] /(1.16 [mol kg^{-1}] × 1.04) = 2.1. This value is significantly higher than that required for spontaneous crystallization of both the stable β-form and metastable α-form (SS > 1.1 for β-form, SS > 1.2 for α-form; see Supplementary Note 6 and Supplementary Fig. 6), demonstrating that laser trapping induces a highly supersaturated state prior to nucleation.

It may seem surprising that laser trapping can induce such a high degree of supersaturation. Still, this phenomenon has been observed in previous studies on other amino acid and protein solutions[29,33,41–43]. It is important to note that the nucleation rate (J) is governed by the magnitude of the logarithm of supersaturation (ln(SS)) and the surface free energy of the growing nucleus (σ), as follows[44,45].

$$J \propto \exp\left(-\frac{16\pi\sigma^3 v^2}{3k_B{}^3T^3(\ln(SS))^2}\right) \quad (1)$$

where v is the volume of L-Cys molecules, k_B is the Boltzmann constant, and T is the temperature. While the supersaturation (SS) of the metastable form is generally smaller than that of the stable form, the values of ln(SS) are nearly equal for both polymorphs with increasing supersaturation[46]. Therefore, under conditions where supersaturation is sufficiently high for both polymorphs, the magnitude of the surface free energy (σ) determines the relative nucleation rates of the two polymorphs. Indeed, σ of the metastable phase is generally smaller than that of the stable phase, regardless of supersaturation. This is related to the higher enthalpy of the stable phase, which arises from stronger intermolecular interactions and more efficient packing within the crystal lattice. These stronger interactions stabilize the crystal structure but also increase the energy required to form a new surface, thus resulting in a higher surface free energy. Consequently, the nucleation rate of the metastable phase is higher than that of the stable phase under highly supersaturated conditions, leading to the preferential crystallization of the metastable phase. This could explain the exclusive crystallization of the metastable α-form upon CW laser trapping.

Effects of HRR fs laser on L-Cys crystallization

In the preceding section, we observed that CW laser irradiation consistently resulted in the crystallization of the α-form of L-Cys despite adjusting parameters such as laser intensity and solution concentration. This observation led us to hypothesize that alternative laser-based perturbations might be required to induce the crystallization of the β-form. To explore this possibility, we employed a focused HRR fs laser, which not only induces laser trapping but also causes additional phenomena such as laser ablation[30,31]. Figure 4 and Movie S2 show the representative crystallization behavior of L-Cys under HRR fs laser trapping. This experiment also employed the unsaturated L-Cys/D_2O solution with SS = 0.84. No apparent change was observed immediately after the laser irradiation. After half an hour of irradiation, bubbles were suddenly generated at the laser focus ($t = 1665$ s). During bubble generation, small crystals (indicated by a red circle in the figure) were repeatedly produced and dissolved around the laser focus. Suddenly, rectangular crystals (indicated by green arrows in the figure) were yielded around the laser focus ($t = 1675$ s). These rectangular crystals grew substantially with continued laser irradiation. When the growing crystals were trapped at the laser focus, they underwent ablation, resulting in poly-crystallization ($t = 1680$ s). Due to the unsaturated nature of the bulk solution, the obtained crystals gradually dissolved after the laser was turned off. However, by carefully removing the upper glass of the sample cell, we could preserve the crystals for several minutes, allowing us to measure their Raman spectra. Surprisingly, Raman spectroscopy confirmed that these rectangular crystals correspond to the stable phase of β-form,

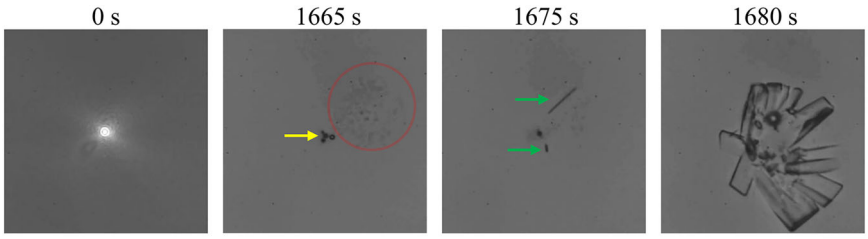

Fig. 4 | Dynamics of HRR fs laser trapping-induced L-Cys crystallization. Evolution of L-Cys crystallization under HRR fs laser trapping. The laser intensity was maintained at 120 MW cm^{-2}. Yellow arrows denote laser-induced bubbles, while green arrows highlight the emergence of stick-like crystals. Thin crystals are encircled in red. The scale bar corresponds to 20 μm.

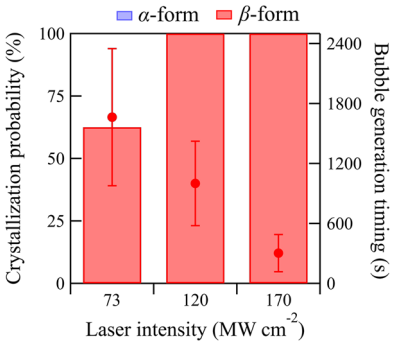

Fig. 5 | Impact of HRR fs laser trapping on L-Cys crystallization. Dependence of crystallization probability and bubble generation timing on laser intensity of HRR fs laser. Linearly polarized light was used as the trapping light source. The stable phase crystal was formed after ~10 s to ~10 min from bubble generation. Eight samples were tested in each condition. To properly evaluate induction time tendency, we assigned a value of 40 min to trials without crystal nucleation at 73 MW cm^{-2}. The error bars represent the standard deviation.

which was never observed with CW laser trapping. Due to their limited size, we were unable to characterize the small crystals that formed prior to β-form crystallization using Raman spectroscopy. Nevertheless, we employed alternative methods to determine that these crystals were likely the α-form, as detailed in the next section.

To examine the impact of HRR fs laser irradiation on the crystallization behavior of L-Cys, we investigated the dependence of eventual polymorphism, crystallization probability, and bubble generation timing on the intensity of the linearly polarized laser. The results are summarized in Fig. 5. Crystals always appeared at 120 and 170 MW cm^{-2}, while some trials failed at 73 MW cm^{-2}. The bubble generation timing was significantly accelerated with increasing laser intensity ($H = 14$, $P = 0.08\%$). While such crystallization behavior is similar to that of the CW laser (Fig. 2), the HRR fs laser irradiation always produced the stable phase of β-form eventually. This result underscores that not only laser trapping but also additional phenomena characteristic of HRR fs laser contributed to the generation of β-form.

We now discuss the crystallization and polymorphism mechanism of L-Cys by HRR fs laser irradiation. Unlike the case of CW laser irradiation, continued irradiation with HRR fs laser suddenly produces bubbles at the laser focus (Fig. 4, $t = 1665$ s). Such bubble generation has also been observed in the experiments on HRR fs laser trapping-induced crystallization using other amino acid solutions[30,31]. This phenomenon can be explained as follows: the focused irradiation with an HRR fs laser induces a concentration increase at the laser focus due to its laser trapping effect[47,48]. As the concentration is increased, the multiphoton absorption by solutes is enhanced due to the considerably higher peak intensity of the HRR fs laser (≥7.6 TW cm^{-2}) compared to the CW laser (≤170 MW cm^{-2})[49,50]. When the concentration reaches a certain level, the multiphoton absorption triggers laser ablation of the solution, producing bubbles[51]. These generated bubbles may correspond to cavitation bubbles that are often produced by irradiation with ultrashort laser pulses[49]. Indeed, it has been reported that bubble generation by laser ablation of solutions can induce crystal nucleation[7,52]. As for its mechanism, several studies have proposed that local concentration increase and/or heterogeneous nucleation at the bubble surface plays an important role in crystal nucleation by laser ablation[53–61]. The preferential nucleation of the small α-form crystals (Fig. 4, $t = 1665$ s, red circle) can be attributed to the localized increase in solute concentration induced by laser trapping and the subsequent generation of cavitation bubbles. This localized concentration increase leads to a high degree of supersaturation, favoring the nucleation of the α-form, which is characterized by lower surface free energy. As the α-form crystals grow, solute molecules are consumed, leading to a decrease in the supersaturation level within the vicinity of the laser focus. With decreasing supersaturation, the values of ln(SS) in Eq.1 are no longer comparable between the two polymorphs, leading to an increase in the nucleation rate of the stable form. Consequently, subsequent bubble generation events within this region of reduced supersaturation promote the nucleation of the β-form polymorph. This phenomenon exemplifies the delicate interplay between supersaturation and surface free energy in determining the polymorphic outcome of crystallization processes. The nucleation rate (Eq. 1) is initially dominated by the surface free energy (σ) due to highly supersaturated conditions, resulting in the crystallization of the metastable α-form via laser-induced bubbles. As the number of metastable α-form crystals increased, the supersaturation (SS) influenced the nucleation rate due to a decrease in supersaturation, eventually leading to the stable β-form crystallization. In fact, such a conversion from metastable polymorph to stable polymorph has also been observed in HRR fs laser trapping of L-phenylalanine[30].

Selective manipulation of polymorphs by the combination of CW laser and HRR Fs laser

The results presented in the preceding sections demonstrate that the eventual polymorph of L-Cys can be controlled by selecting the appropriate laser irradiation mode: CW laser irradiation consistently yields the α-form, while HRR fs laser irradiation ultimately produces the β-form. Building upon these findings, we explored the possibility of achieving dynamic control over the eventual number of crystals and the resulting polymorph by strategically combining CW and HRR fs laser irradiation.

For this purpose, we designed an experiment where we switched between CW and HRR fs laser irradiation during crystal growth. As shown in the leftmost image in Fig. 6, we first irradiated the HRR fs laser at 170 MW cm^{-2} into the L-Cys solution until bubble generation was observed at the laser focus. Immediately confirming the bubble generation, we switched to CW laser irradiation. Contrary to the case of CW laser trapping alone (Fig. 1), this change in irradiation mode immediately led to the continued growth of the large single α-form crystal (~200 μm) (the upper path in Fig. 6 and Supplementary Movie 3). This result indicates that switching to CW laser irradiation before β-form crystallization by the subsequent HRR fs laser irradiation can promote the growth of α-form crystals. This result further supports our interpretation that the small crystals observed before β-form crystallization (Fig. 4, $t = 1665$ s, red circle) are α-form crystals. Furthermore, we confirmed that re-switching to HRR fs laser irradiation after sufficient growth of the α-form crystal eventually still led to the formation of the β-form (Supplementary Fig. 7 and Supplementary Movie 4). Specifically, re-switching to HRR fs laser initially induced

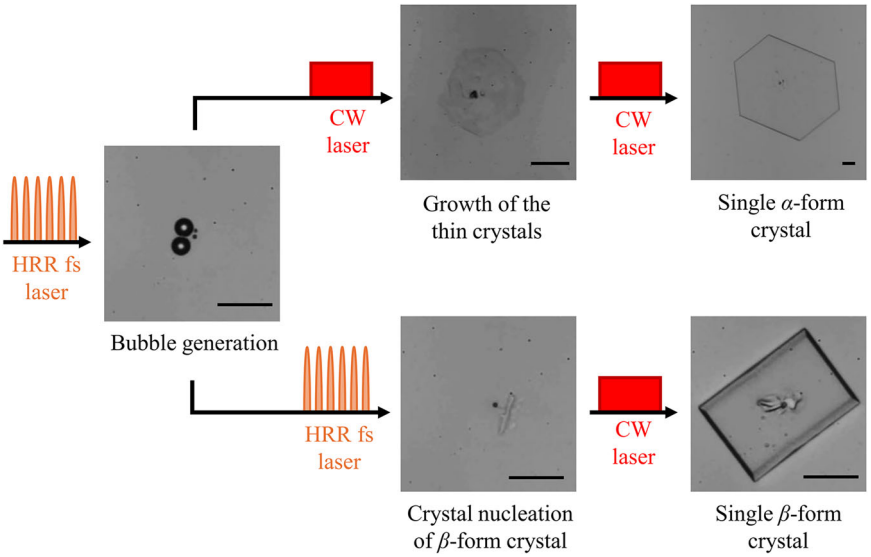

Fig. 6 | Combination of CW laser and HRR fs laser. Polymorph control of L-Cys by sequential irradiation with CW and HRR fs lasers. The scale bars represent 20 μm.

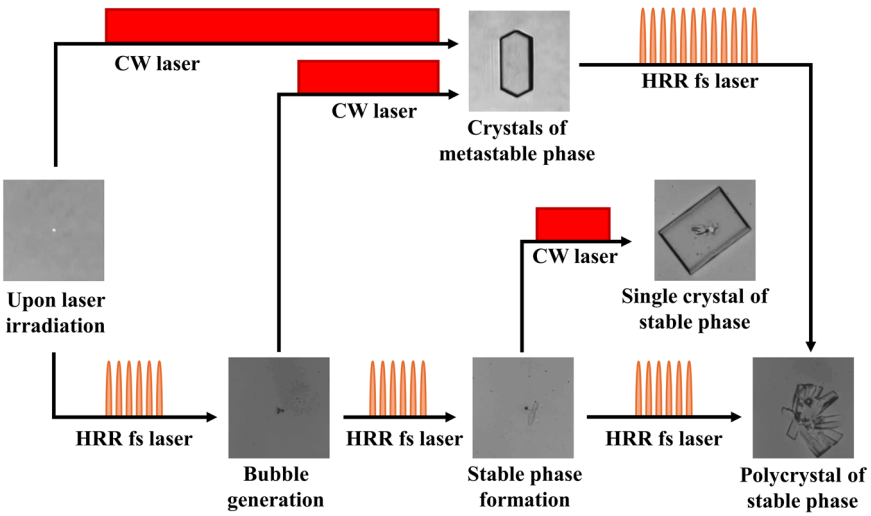

Fig. 7 | Summary of polymorphic control of L-Cys crystals demonstrated in this study. Polymorph control of L-Cys crystals achieved by CW and HRR fs laser trapping.

etching of the crystal's surface with generating bubbles. Approximately 2 min after re-switching to the HRR fs laser, the β-form crystals suddenly appeared around the laser focus. This observation underscores the role of HRR fs laser irradiation in inducing β-form crystallization.

The combination of CW laser and HRR fs laser also offers another advantage. Activating the CW laser immediately after the crystallization of the β-form resulted in single-crystal growth without poly-crystallization (the bottom path in Fig. 6 and Supplementary Movie 5). This precise control over single-crystal growth is challenging to achieve with the HRR fs laser alone, as demonstrated in Fig. 4. Thus, precise spatial and temporal manipulation of CW and HRR fs laser irradiation enables the preparation of single L-Cys crystals with the desired polymorph. This technique offers a level of control over the crystallization and polymorphism process, allowing for the targeted production of specific polymorphs.

Conclusions

This study has delved into the selective manipulation of L-Cys polymorphism, revealing the remarkable ability of focused laser irradiation to guide the polymorphism selectively. We have demonstrated that CW laser irradiation consistently yields the metastable α-form, while HRR fs laser irradiation favors the stable β-form. This intriguing divergence stems from the distinct mechanisms triggered by each laser type. CW laser irradiation generates a highly supersaturated state, promoting the rapid formation of the metastable α-form. Conversely, HRR fs laser irradiation induces localized concentration increases followed by bubble generation, ultimately promoting the formation of the stable β-form. These polymorphic behaviors, illustrated based on the solubility curve, are summarized in Supplementary Fig. 8.

Taking this a step further, we achieved dynamic control over the crystallization pathway by strategically alternating between CW and HRR fs laser irradiation. This approach, visually summarized in Fig. 7, allowed us to achieve favorable results in crystal engineering, such as growing large single crystals of the α-form and preventing polycrystallization of the β-form. The implications of this work extend far beyond L-Cys. We anticipate that the precise control of crystal polymorphs achieved by harnessing the interplay of laser parameters and material responses will find applications in diverse fields where crystal polymorphism is crucial, including pharmaceutics and optoelectronics.

Methods

Sample preparation

L-Cys (≥99%, Sigma-Aldrich) was used as received without further purification. L-Cys crystals were completely dissolved in deuterium oxide (D_2O) by stirring at 70 °C for 15 min. D_2O was chosen as the solvent instead

of H_2O to minimize temperature increases caused by the near-infrared CW laser irradiation. The temperature elevation coefficients (thermal absorption coefficients) at 1064 nm are reportedly 22–24 and 1–2 K W^{-1} for H_2O and D_2O, respectively[62]. The solution was then cooled and incubated at room temperature (~25 °C) for 1 h. For the laser experiments, a 15 μL aliquot of the solution was placed into a custom-made, hydrophilized sample cell consisting of a cover glass and a glass ring (Supplementary Fig. 9). After pouring the solution into the handmade cell, it was sealed with another cover glass. The solution height was measured to be 160 ± 10 μm. Because prolonged incubation of L-Cys in the sample solutions (e.g., 1 day) can lead to the precipitation of "cystine" (Supplementary Fig. 10) due to cysteine oxidization[63], solutions were always used within 5 h of preparation. The sample cell was mounted on the microscope stage for subsequent laser experiments.

Optical setup for CW laser trapping combined with Raman spectroscopic system

The optical setup for the combined CW laser trapping and Raman spectroscopic system is shown in Supplementary Fig. 11a. A near-infrared CW laser (λ = 1064 nm) emitted from Nd^{3+}:YVO_4 laser system (J201-BL-106C, Spectra-Physics) was employed for laser trapping. The laser beam was expanded and collimated using two convex lenses with a focal length (f) of 100 and 200 mm, and then directed into a microscope (Eclipse Ti, Nikon). The laser beam was focused at the air/solution interface of the sample solution through an objective lens with a numerical aperture (NA) of 0.90 (×60, UPLFLN60X, Olympus). The laser power was adjusted using a half-wave plate and a polarizing beam splitter. The focal radius was estimated to be ~720 nm based on the Rayleigh criterion (×0.61, λ/NA), and this value was used to determine the laser intensity. The microscopic image through the objective lens was captured by a CCD camera capable of detecting visible to near-infrared light (CV-S3200, Jai).

For Raman spectroscopy, a green CW laser (λ = 532 nm, Millennia Pro s-Series 10 sJS, Spectra-Physics) served as the excitation source. Similar to the trapping laser, the excitation laser beam was expanded and collimated using convex lenses (f = 100 and 200 mm). The excitation laser was converted to circularly polarized light to minimize the influence of molecular alignment in the crystal on the Raman scattering measurements. The scattered light was collected by a spectrometer (Shamrock, Andor) through an optical fiber (SR-OPT-8020, Andor) and detected by a cooled CCD camera (iDus, Andor). A notch filter positioned before the fiber blocked Rayleigh scattering and reflected light. Spectral analysis was performed using SOLIS software (Andor).

Optical setup for HRR fs laser trapping and CW laser trapping

The optical setup for HRR fs laser trapping and CW laser trapping is illustrated in Supplementary Fig. 11b. We utilized a mode-lock Ti:Sapphire laser system (Tsunami, Spectra-Physics) to generate HRR fs laser pulses. This system was pumped by a green CW laser (λ = 532 nm, Millennia-eV, Spectra-Physics) and produced pulses with a central wavelength of 800 nm, a pulse duration of 120 fs, and a repetition rate of 80 MHz. To ensure optimal beam quality, the laser pulses were expanded and collimated using a concave lens (f = −150 mm) and a convex lens (f = 250 mm). In addition to the HRR fs laser, we incorporated a near-infrared CW laser (λ = 1064 nm, Nd^{3+}: YVO_4, MATRIX 1064-10-CW, Coherent) into the setup. This CW laser beam was also expanded and collimated, this time using two convex lenses (f = 100 mm and 200 mm). Both laser beams were then introduced to the inverted microscope (IX71, Olympus) and focused at the air/solution interface using the objective lens (×60, NA = 0.90). The focal radius of the HRR fs laser was estimated to be 540 nm. Finally, the polymorphs generated by laser irradiation were characterized using the optical system described in the previous section.

Data availability

The data that support the findings of this study are available from the corresponding author upon reasonable request.

Received: 6 January 2025; Accepted: 7 May 2025;
Published online: 16 May 2025

References

1. Brittain, H. G. Polymorphism in pharmaceutical solids. *Drugs Pharm. Sci.* **95**, 183–226 (1999).
2. Morissette, S. L. et al. High-throughput crystallization: polymorphs, salts, co-crystals and solvates of pharmaceutical solids. *Adv. Drug Deliv. Rev.* **56**, 275–300 (2004).
3. Diao, Y. et al. Understanding polymorphism in organic semiconductor thin films through nanoconfinement. *J. Am. Chem. Soc.* **136**, 17046–17057 (2014).
4. Nogueira, B. A., Castiglioni, C. & Fausto, R. Color polymorphism in organic crystals. *Commun. Chem.* **3**, 34 (2020).
5. Liu, G., Gou, R., Li, H. & Zhang, C. Polymorphism of energetic materials: a comprehensive study of molecular conformers, crystal packing, and the dominance of their energetics in governing the most stable polymorph. *Cryst. Growth Des.* **18**, 4174–4186 (2018).
6. Kitamura, M. Controlling factor of polymorphism in crystallization process. *J. Cryst. Growth* **237-239**, 2205–2214 (2002).
7. Yoshikawa, H. Y. et al. Laser ablation for protein crystal nucleation and seeding. *Chem. Soc. Rev.* **43**, 2147–2158 (2014).
8. Alexander, A. J. & Camp, P. J. Non-photochemical laser-induced nucleation. *J. Chem. Phys.* **150**, 040901 (2019).
9. Sugiyama, T. & Wang, S.-F. Manipulation of nucleation and polymorphism by laser irradiation. *J. Photochem. Photobiol. C* **52**, 100530 (2022).
10. Korede, V. et al. A review of laser-induced crystallization from solution. *Cryst. Growth Des.* **23**, 3873–3916 (2023).
11. Garetz, B. A., Matic, J. & Myerson, A. S. Polarization switching of crystal structure in the nonphotochemical light-induced nucleation of supersaturated aqueous glycine solutions. *Phys. Rev. Lett.* **89**, 175501 (2002).
12. Li, W. et al. Non-photochemical laser-induced nucleation of sulfathiazole in a water/ethanol mixture. *Cryst. Growth Des.* **16**, 2514–2526 (2016).
13. Ikni, A. et al. Experimental demonstration of the carbamazepine crystallization from non-photochemical laser-induced nucleation in acetonitrile and methanol. *Cryst. Growth Des.* **14**, 3286–3299 (2014).
14. Sun, X., Garetz, B. A. & Myerson, A. S. Polarization switching of crystal structure in the nonphotochemical laser-induced nucleation of supersaturated aqueous L-histidine. *Cryst. Growth Des.* **8**, 1720–1722 (2008).
15. Ikeda, K. et al. Selective crystallization of the metastable phase of indomethacin at the interface of liquid/air bubble induced by femtosecond laser irradiation. *Appl. Phys. Express* **8**, 045501 (2015).
16. Tsuri, Y. et al. Crystallization of aspirin form II by femtosecond laser irradiation. *Appl. Phys. Express* **12**, 015507 (2018).
17. Wang, S. et al. Polymorph-controlled crystallization of acetaminophen through femtosecond laser irradiation. *Cryst. Growth Des.* **19**, 3265–3271 (2019).
18. Yu, J., Yan, J. & Jiang, L. Crystallization of polymorphic sulfathiazole controlled by femtosecond laser-induced cavitation bubbles. *Cryst. Growth Des.* **21**, 3202–3210 (2021).
19. Barber, E. R., Ward, M. R., Ward, A. D. & Alexander, A. J. Laser-induced nucleation promotes crystal growth of anhydrous sodium bromide. *CrystEngComm* **23**, 8451–8461 (2021).
20. Takahashi, H. et al. Pseudopolymorphism of sodium acetate in supersaturated aqueous solution induced by focused irradiation with ultrashort laser pulses. *J. Phys. Chem. C* **128**, 11046–11053 (2024).
21. Ashkin, A. History of optical trapping and manipulation of small-neutral particle, atoms, and molecules. *IEEE J. Sel. Top. Quantum Electron.* **6**, 841–856 (2000).
22. Neuman, K. C. & Block, S. M. Optical trapping. *Rev. Sci. Instrum.* **75**, 2787–2809 (2004).

23. Maragò, O. M., Jones, P. H., Gucciardi, P. G., Volpe, G. & Ferrari, A. C. Optical trapping and manipulation of nanostructures. *Nat. Nanotechnol.* **8**, 807–819 (2013).
24. Masuhara, H. & Yuyama, K.-i Optical force-induced chemistry at solution surfaces. *Annu. Rev. Phys. Chem.* **72**, 565–589 (2021).
25. Sugiyama, T., Yuyama, K.-i & Masuhara, H. Laser trapping chemistry: from polymer assembly to amino acid crystallization. *Acc. Chem. Res.* **45**, 1946–1954 (2012).
26. Yuyama, K.-i, Rungsimanon, T., Sugiyama, T. & Masuhara, H. Selective fabrication of α- and γ-polymorphs of glycine by intense polarized continuous wave laser beams. *Cryst. Growth Des.* **12**, 2427–2434 (2012).
27. Wu, C.-S., Hsieh, P.-Y., Yuyama, K.-i, Masuhara, H. & Sugiyama, T. Pseudopolymorph control of L-phenylalanine achieved by laser trapping. *Cryst. Growth Des.* **18**, 5417–5425 (2018).
28. Shih, T.-W. et al. Optical trapping-induced new polymorphism of β-cyclodextrin in unsaturated solution. *Cryst. Growth Des.* **21**, 6913–6923 (2021).
29. Takahashi, H., Yoshikawa, H. Y. & Sugiyama, T. Raman spectroscopic study of concentration dynamics in glycine crystallization achieved by optical trapping. *J. Photochem. Photobiol. A* **456**, 115845 (2024).
30. Wu, C.-S., Yoshikawa, H. Y. & Sugiyama, T. Bidirectional polymorphic conversion by focused femtosecond laser irradiation. *Jpn. J. Appl. Phys.* **59**, SIIH02 (2020).
31. Wang, W.-C., Wang, S.-F. & Sugiyama, T. L-serine polymorphism controlled by optical trapping with high-repetition-rate femtosecond laser pulses. *J. Chin. Chem. Soc.* **69**, 200–210 (2022).
32. Barber, E. R., Ward, M. R. & Alexander, A. J. The role of cavitation and gas bubbles in the non-photochemical laser-induced nucleation of sodium acetate. *CrystEngComm* **26**, 3634–3642 (2024).
33. Hanasaki, I., Okano, K., Yoshikawa, H. Y. & Sugiyama, T. Spatiotemporal dynamics of laser-induced molecular crystal precursors visualized by particle image diffusometry. *J. Phys. Chem. Lett.* **10**, 7452–7457 (2019).
34. Clemente Plaza, N., Reig García-Galbis, M. & Martínez-Espinosa, R. M. Effects of the usage of L-cysteine (L-Cys) on human health. *Molecules* **23**, 575 (2018).
35. Moggach, S. A. et al. High-pressure polymorphism in L-cysteine: the crystal structures of L-cysteine-III and L-cysteine-IV. *Acta Crystallogr. B* **62**, 296–309 (2006).
36. Minkov, V. S., Goryainov, S. V., Boldyreva, E. V. & Görbitz, C. H. Raman study of pressure-induced phase transitions in crystals of orthorhombic and monoclinic polymorphs of L-cysteine: dynamics of the side chain. *J. Raman Spectrosc.* **41**, 1748–1758 (2010).
37. Parker, S. F. Assignment of the vibrational spectrum of L-cysteine. *Chem. Phys.* **424**, 75–79 (2013).
38. Liu, S.-F., Wang, Y. & Lin, L. Laser-induced crystallization of amino acids through the coordinated effect of optical forces and Marangoni convection. *J. Phys. Chem. A* **128**, 11055–11060 (2024).
39. Kruskal, W. H. & Wallis, W. A. Use of ranks in one-criterion variance analysis. *J. Am. Stat. Assoc.* **47**, 583–621 (1952).
40. Han, J. et al. Determination and correlation of the solubility of L-cysteine in several pure and binary solvent systems. *J. Chem. Eng. Data* **65**, 2649–2658 (2020).
41. Yuyama, K.-i, Sugiyama, T. & Masuhara, H. Millimeter-scale dense liquid droplet formation and crystallization in glycine solution induced by photon pressure. *J. Phys. Chem. Lett.* **1**, 1321–1325 (2010).
42. Gowayed, O. Y. et al. Dynamic light scattering study of a laser-induced phase-separated droplet of aqueous glycine. *J. Phys. Chem. B* **125**, 7828–7839 (2021).
43. Chen, T., Toyouchi, S. & Sugiyama, T. Spectroscopic analysis of concentration dynamics and crystallization of hen egg-white lysozyme under optical trapping conditions. *J. Phys. Chem. C.* **127**, 23340–23348 (2023).
44. Markov, I. V. *Crystal Growth for Beginners: Fundamentals of Nucleation, Crystal Growth and Epitaxy* (World Scientific Publishing, 2003).
45. Kitamura, M. Polymorphism in adductive crystallization of Ni-complex in the presence of 1-methylnaphthalene. *J. Chem. Eng. Jpn.* **21**, 589–595 (1988).
46. Verma, V. & Hodnett, B. K. A basis for the kinetic selection of polymorphs during solution crystallization of organic compounds. *CrystEngComm* **20**, 5551–5561 (2018).
47. Jiang, Y., Narushima, T. & Okamoto, H. Nonlinear optical effects in trapping nanoparticles with femtosecond pulses. *Nat. Phys.* **6**, 1005–1009 (2010).
48. Usman, A., Chiang, W.-Y. & Masuhara, H. Optical trapping and polarization-controlled scattering of dielectric spherical nanoparticles by femtosecond laser pulses. *J. Photochem. Photobiol. A* **234**, 83–90 (2012).
49. Vogel, A., Noack, J., Hüttman, G. & Paltauf, G. Mechanisms of femtosecond laser nanosurgery of cells and tissues. *Appl. Phys. B* **81**, 1015–1047 (2005).
50. Vogel, A., Linz, N., Freidank, S. & Paltauf, G. Femtosecond-laser-induced nanocavitation in water: implications for optical breakdown threshold and cell surgery. *Phys. Rev. Lett.* **100**, 038102 (2008).
51. Vogel, A. & Venugopalan, V. Mechanisms of pulsed laser ablation of biological tissues. *Chem. Rev.* **103**, 577–644 (2003).
52. Soare, A. et al. Crystal nucleation by laser-induced cavitation. *Cryst. Growth Des.* **11**, 2311–2316 (2011).
53. Nakamura, K., Hosokawa, Y. & Masuhara, H. Anthracene crystallization induced by single-shot femtosecond laser irradiation: experimental evidence for the important role of bubbles. *Cryst. Growth Des.* **7**, 885–889 (2007).
54. Yoshikawa, H. Y. et al. Laser energy dependence on femtosecond laser-induced nucleation of protein. *Appl. Phys. A* **93**, 911–915 (2008).
55. Yoshikawa, H. Y. et al. Femtosecond laser-induced nucleation of protein in agarose gel. *J. Cryst. Growth* **311**, 956–959 (2009).
56. Iefuji, N. et al. Laser-induced nucleation in protein crystallization: Local increase in protein concentration induced by femtosecond laser irradiation. *J. Cryst. Growth* **318**, 741–744 (2011).
57. Hidman, N., Sardina, G., Maggiolo, D., Ström, H. & Sasic, S. Numerical frameworks for laser-induced cavitation: Is interface supersaturation a plausible primary nucleation mechanism? *Cryst. Growth Des.* **20**, 7276–7290 (2020).
58. Takahashi, H., Sugiyama, T., Nakabayashi, S. & Yoshikawa, H. Y. Crystallization from glacial acetic acid melt via laser ablation. *Appl. Phys. Express* **14**, 045503 (2021).
59. Tsuri, Y. et al. Effects of pulse duration on laser-induced crystallization of urea from 300 to 1200 fs: impact of cavitation bubbles on crystal nucleation. *Appl. Phys. A* **128**, 1–7 (2022).
60. Nagalingam, N. et al. Laser-induced cavitation for controlling crystallization from solution. *Phys. Rev. Lett.* **131**, 124001 (2023).
61. Takahashi, H. et al. Spatiotemporal control of ice crystallization in supercooled water via an ultrashort laser impulse. *J. Phys. Chem. Lett.* **14**, 4394–4402 (2023).
62. Ito, S., Sugiyama, T., Toitani, N., Katayama, G. & Miyasaka, H. Application of fluorescence correlation spectroscopy to the measurement of local temperature in solutions under optical trapping condition. *J. Phys. Chem. B* **111**, 2365–2371 (2007).
63. Ejgenberg, M. & Mastai, Y. Biomimetic crystallization of L-cystine hierarchical structures. *Cryst. Growth Des.* **12**, 4995–5001 (2012).

Acknowledgements

This work was partly supported by grants from the Japan Science and Technology Agency (JST) through the ACT-X program (No. JPMJAX23DC to HT), Japan Society for the Promotion of Science (JSPS) fellows (Nos. JP22KJ2214 and JP22J21666 to H.T.), and a KAKENHI Grant-in-Aid for Transformative Research Areas (A) "Revolution of Chiral Materials Science using Helical Light Fields" (No. JP22H05138 to T.S.). Additional support was

provided by the JSPS KAKENHI (Nos.: JP24H01138, JP23K18576, JP22H00302, JP22H05423, and JP19KK0128 to H.Y.Y., JP24KK0106 to H.Y.Y. and H.T.), Amada Foundation, and Asahi Glass Foundation. We also acknowledge the support from the National Science and Technology Council (NSTC) of Taiwan (MOST 113-2113-M-A49-023 to TS) and the Center for Emergent Functional Matter Science of National Yang Ming Chiao Tung University from The Featured Areas Research Center Program within the framework of the Higher Education Sprout Project by the Ministry of Education (MOE) of Taiwan (NSTC 111-2634-F-A49-007 to T.S.). Our gratitude also extends to the support from the Japan–Taiwan Exchange Association.

Author contributions

H.T. and T.S. conceptualized the research. H.T. carried out the experiments with guidance from H.Y.Y. and T.S. The first draft of the manuscript was written by H.T. All authors discussed the results and edited the manuscript.

Competing interests

The authors declare no competing interests.

Additional information

Supplementary information The online version contains supplementary material available at https://doi.org/10.1038/s42004-025-01554-7.

Correspondence and requests for materials should be addressed to Hozumi Takahashi or Teruki Sugiyama.

Peer review information *Communications Chemistry* thanks Tetsuo Okutsu and the other anonymous reviewers for their contribution to the peer review of this work.